Available online at www.sciencedirect.com
SCIENCE DIRECT®
Global and Planetary Change 38 (2003) 137–149
GLOBAL AND PLANETARY CHANGE
www.elsevier.com/locate/gloplacha

Simulation of a Scandinavian basin using the diffusion transfer version of ISBA

Florence Habets*, Aaron Boone, Joël Noilhan

Météo-France/Centre National de Recherches Meteorologiques (CNRM), 42 Avenue Coriolis, 31057 Toulouse, France

Received 21 November 2001; received in revised form 21 December 2001; accepted 4 June 2002

Abstract

A brief description of the two-layer frozen soil scheme and the three-layer explicit snow model used by ISBA for the PILPS2(e) experiment is presented, as well as the new soil diffusion scheme of ISBA. This new version of ISBA has a more physical description of the frozen soil processes, and it has been applied in the Torne–Kalix basins where these processes are important. The simulations of the force restore and diffusion version of ISBA (ISBA-FR and ISBA-DF, respectively) are compared to in situ observations of snow height and soil temperature at the Abisko research station, as well as to the observed riverflow at five locations. In terms of riverflow, the ISBA-DF scheme obtained results comparable to the ISBA-FR scheme, with a weakness to simulate the Abisko basin, but a good ability to simulate the Lansjaarv streamflow. However, ISBA-DF compares better than ISBA-FR to the soil temperature observed at the Abisko research station.
© 2003 Elsevier Science B.V. All rights reserved.

Keywords: Torne–Kalix basins; ISBA; diffusion transfer

1. Introduction

The ISBA land surface scheme (Noilhan and Planton, 1989; Noilhan and Mahfouf, 1996) is used in the numerical prediction of and Météo-France, as well as in the Arpege climate model and research mesoscale model MesoNH. Its various applications have lead to new developments, most notably an explicit urban scheme (Masson, 2000), an interactive vegetation scheme (Calvet et al., 1998; Calvet, 2000), a new parameterization of soil freezing (Giard and Bazile, 2000; Boone et al., 1999), snow cover (Boone and Etchevers, 2001), and even a diffusion approach for the soil column heat and water transfer (Boone et al., 1999). ISBA has been coupled to a hydrological model (Habets et al., 1999a; Etchevers et al., 2000), which was also used for the Rhone-AGG experiment (Boone et al., 2001). A tile version of ISBA has been developed in order to explicitly distinguish some heterogeneities in the cell as, for instance, forest from bare soil or irrigated areas. All of these parameterizations can be used optionally, so that the level of complexity can be set according to the purpose of the experiment.

ISBA has participated to the Phase 2(e) of the PILPS2 experiment (Bowling et al., 2003-this issue; Nijssen et al., 2003-this issue), which focuses on the treatment of the cold processes, by studying the

* Corresponding author.
E-mail address: florence.habets@meteo.fr (F. Habets).

0921-8181/03/$ - see front matter © 2003 Elsevier Science B.V. All rights reserved.
doi:10.1016/S0921-8181(03)00016-X

Scandinavian basins of the Torne and Kalix. The three-layer snow scheme (ISBA-ES) and the two-layer frozen scheme of the force-restore version of ISBA (ISBA-FR) were used during this experiment. The results obtained by ISBA-FR, as discussed in Bowling et al. (2003-this issue) and Nijssen et al. (2003-this issue), were acceptable in terms of simulation of the overall riverflows and snow. However, some problems in terms of phasing of the riverflow for a part of the basin were detected. The Torne–Kalix basin is subject to frozen soil and even permafrost in the higher parts of the basin (Bowling et al., 2003-this issue). The description of the frozen soil in ISBA-FR is limited due to the depth represented by the deep soil temperature (see Section 2.2). Thus, the frozen soil is limited to about 30 cm, which certainly leads to unrealistic simulation of the frozen depth and soil temperature. The purpose of this article is to improve the simulation of the frozen soil of the Torne–Kalix basin using the diffusion version of ISBA, which allows to solve the thermal profile of the soil. The description of the main part of ISBA-FR and ISBA-DF, as well as the explicit snow-scheme ISBA-ES, are briefly presented in Section 2, and the comparison of ISBA-DF and IBSA-FR over the PILPS2e domain is presented Section 3.

2. The ISBA surface scheme

2.1. ISBA energy budget

Over the snow-free part of the mesh, the net radiation, R_n, is the sum of the intercepted shortwave, R_G, and long-wave, R_A, radiation, less the long-wave blackbody emission of the surface. The surface flux components can be summarized as:

$$R_n = R_G(1-\alpha) + \epsilon(R_A - \sigma T_s^4) = H + G + \mathrm{LE} \quad (1)$$

$$H = \rho_a C_p C_H V_a (T_s - T_a) \quad (2)$$

$$\mathrm{LE} = L_v(E_{gl} + E_v) + L_s(E_{gi}) \quad (3)$$

$$E_{gl} = (1-\mathrm{froz})(1-\mathrm{veg})\rho_a C_H V_a [h_u q_{sat}(T_s) - q_a] \quad (4)$$

$$E_{gi} = \mathrm{froz}(1-\mathrm{veg})\rho_a C_H V_a [h_{ui} q_{sat}(T_s) - q_a] \quad (5)$$

$$E_v = \mathrm{veg}\rho_a C_H V_a h_v [q_{sat}(T_s) - q_a] \quad (6)$$

where LE, H, and G are the latent, sensible, and ground heat flux, E_{gl} and E_{gi} are the bare soil evaporation and sublimation, and E_v is the evapotranspiration. The veg parameter is the fraction of the vegetation cover, and froz is the fraction of frozen soil water that is set to froz $= w_{i1}/(w_{i1} + w_{l1})$, where w_{i1} and w_{l1} represent the ice and liquid soil water content of the surface layer, respectively (see Appendix A for the other variables).

When the explicit three-layer snow scheme (Boone and Etchevers, 2001) is used, there is a distinct energy budget for the snowpack (see Section 2.4), and the total net radiation is the sum of the snow and soil–vegetation net radiation:

$$R_{nt} = (1-p_n)R_n + p_n R_{nsnow} \quad (7)$$

where p_n represents the surface snow fraction. If the composite snow scheme (Douville et al., 1996) is used, there is just one energy budget, and the surface temperature, T_s, corresponds to the composite snow–soil–vegetation temperature, and the latent heat flux includes a snow sublimation component (E_{snow}).

2.2. ISBA force restore

The force-restore version of ISBA now includes a two-layer parameterization of soil-freezing (Boone et al., 2000), and a third hydrological layer that represents the soil column below the root zone (Boone et al., 1999), which leads to seven prognostic variables. Compared to the original version of ISBA (Noilhan and Planton, 1989), the inclusion of a phase change between liquid water and ice (Φ_{wi1} and Φ_{wi2} for the surface and root layer, respectively, see Section 2.3) modifies the evolution of the surface (T_s) and deep (T_2) soil temperatures, as well as the evolution of the

liquid water in the surface and root zone reservoirs (w_{l1} and w_{l2}):

$$\frac{\partial T_s}{\partial t} = (1-\delta_{snow})\left(C_T[R_n - H - LE - L_f \times (\Phi_{snow} - \Phi_{wi1})] - \frac{2\pi}{\tau}(T_s - T_2)\right) + \delta_{snow} G_{snowgrnd} \quad (8)$$

$$\frac{\partial T_2}{\partial t} = \frac{1}{\tau}(T_s - T_2) + C_G L_f \Phi_{wi2} \quad (9)$$

$$\frac{\partial w_{l1}}{\partial t} = \frac{C_1}{d_1 \rho_w}(P_g - E_{gl}) - \frac{1}{d_1 \rho_w}\Phi_{wi1} - \frac{C_2}{\tau} \times (w_{l1} - w_{l1eq})(w_{lmin} \le w_{l1} \le w_{sat} - w_{i1}) \quad (10)$$

$$\frac{\partial w_{l2}}{\partial t} = \frac{1}{\rho_w d_2}(P_g - E_{gl} - E_{tr} - \Phi_{wi2}) - K_2 - D_2 \quad (11)$$

$$\frac{\partial w_{l3}}{\partial t} = \frac{d_2}{(d_3 - d_2)}(K_2 + D_2) - K_3 \quad (12)$$

$$\frac{\partial w_{i1}}{\partial t} = \frac{1}{d_1 \rho_w}(\Phi_{wi1} - E_{gi}) \qquad (0 \le w_{i1} \le w_{sat} - w_{lmin}) \quad (13)$$

$$\frac{\partial w_{i2}}{\partial t} = \frac{1}{(d_2 - d_1)\rho_w}\Phi_{wi2} \qquad (0 \le w_{i2} \le w_{sat} - w_{lmin}) \quad (14)$$

The surface temperature has a different meaning depending on which snow scheme is used. If the single-layer snow scheme is used, the surface temperature corresponds to the soil–vegetation–snow temperature. Then the coefficient δ_{snow} is set to zero, and the coefficient C_T includes the snow thermal properties. If the explicit snow scheme is used, T_s represents the snow–free soil–vegetation surface temperature, and the coefficient δ_{snow} is equal to the snow fraction, p_n. The additional term $G_{snowgrnd}$ represents the energy flux between the soil and the snowpack, and is presented in Section 2.4.

The soil water diffusion (D) and drainage (K) terms are:

$$K_2 = \frac{C_3}{\tau}\frac{d_3}{d_2}\max[\text{wdrain}, (w_{l2} - w_{fc})] \quad (15)$$

$$K_3 = \frac{C_3}{\tau}\frac{d_3}{d_3 - d_2}\max[\text{wdrain}, (w_{l3} - w_{fc})] \quad (16)$$

$$D_2 = \frac{C_4}{\tau}(w_{l2} - w_{l3}) \quad (17)$$

Some baseflow generation is allowed even when the cell-averaged soil moisture is below field capacity, w_{fc}, in order to take into account some spatial heterogeneities, and especially, some small aquifers (associated for instance to a river bed). The baseflow is proportional to a prescribed value wdrain, and the default value is set to 0.001 m^3/m^3, which corresponds to a minimal baseflow of 0.1 mm/day for a clay soil (Habets et al., 1999b; Etchevers et al., 2000). A subgrid runoff scheme, which allows the generation of surface runoff even when the soil is not saturated, is taken into account by the way of the variable infiltration capacity scheme (Wood et al., 1992; Habets et al., 1999a).

The force-restore coefficients have been modified to take into account the effect of soil ice on the soil thermal properties (C_T) and soil water properties, assuming that an icy soil acts like a dryer soil (C_1 C_2, and C_4; Boone et al., 2000).

As the deep soil temperature is representative of a limited soil depth, soil freezing has to be limited to a maximum soil depth zfmax which is approximated using the penetration depth of the thermal wave associated with T_2 (Boone et al., 2000).

This limitation is released if the multilayer diffusion scheme ISBA-DF is used, since the soil temperature, the soil ice, and the liquid water are computed for each layer.

2.3. ISBA diffusion

The ISBA-DF soil module offers some new possibilities: the computation of a vertical profile of the temperature, liquid water, and ice content, over as many layers as needed, and the ability to take into account the vertical variability of the soil texture and root zone profile, if this kind of information is available.

This scheme has already been applied successfully over a fallow site (Boone, 2000) and an agricultural site (Boone et al., 1999), where in situ data collected at several depths allowed a validation of the simulation.

The heat and mass transfer equations of the ISBA-DF model are:

$$c_g \frac{\partial T_j}{\partial t} = \frac{\partial G_i}{\partial z} + \Phi_j = \frac{\partial}{\partial z}\left(\lambda \frac{\partial T_j}{\partial z}\right) + \Phi_j \tag{18}$$

$$\frac{\partial w_{l_j}}{\partial t} = -\frac{\partial F_j}{\partial z} - \frac{\Phi_j}{L_f \rho_w} - \frac{S_l}{\rho_w} \qquad (w_{lmin} \le w_{l_j} \le w_{sat}) \tag{19}$$

$$\frac{\partial w_{i_j}}{\partial t} = \frac{\Phi_j}{L_f \rho_w} - \frac{S_i}{\rho_w} \qquad (0 \le w_{i_j} \le w_{sat} - w_{lmin}) \tag{20}$$

where Φ_j is the energy flux due to phase transformation between liquid and solid water, F_j is the vertical water flux due to drainage and diffusion, and S_l and S_i are liquid water source or sink term due to liquid/vapor (E_g, E_{tr}) and ice/vapor (E_{gi}) phase transformations, respectively.

The vertical soil water flux is parameterized following Darcy's law:

$$F = -k \frac{\partial}{\partial z}(\Psi + z) - D_{v\Psi} \frac{\partial \Psi}{\partial z} \tag{21}$$

where $D_{v\Psi}$ is the vapor conductivity (Braud et al., 1993), Ψ is the soil water potential, and k is the hydraulic conductivity. These variables are linked to the soil water content through the expressions (Brooks and Corey, 1966; Clapp and Hornberger, 1978):

$$\Psi = \Psi_{sat}(w_l / w_{sat})^{-b} \tag{22}$$

$$k = k_{sat}(w_l / w_{sat})^{2b+3} \tag{23}$$

The energy flux of phase transformation Φ for each layer depends on the soil layer temperature, and also on the ice (or liquid) water content:

$$\Phi_j = \frac{1}{\tau_i} \times \begin{cases} \min[\mu_j c_i (T_f - T_j), (w_{l_j} - w_{min}) L_f \rho_w] & (T_j \le T_f) \\ -\min[\mu_j c_i (T_j - T_f), w_{i_j} L_f \rho_w] & (T_j > T_f) \end{cases} \tag{24}$$

μ_j is an efficiency term that simulates the fact that it is easier to freeze a layer which is mostly liquid, or to melt the ice of a layer with a large frozen water content (Boone et al., 2000). In addition, when it is freezing, the maximum liquid water content allowable is limited using the relation between water potential and temperature from Fuchs et al. (1978) (i.e. $\mu_j = 0$ when $w_{l_j} > w_{ljmax}$).

The soil water stress of the plant used to compute the transpiration E_{tr} is now computed using the average of the liquid water content over the root zone layer (d_2) in proportion to the root fraction of each layer.

2.4. ISBA-ES: explicit snow scheme

A new three-layer snow scheme has been developed (Boone and Etchevers, 2001) to take into account additional processes in comparison to the composite snow scheme of Douville et al. (1996). ISBA-ES is an independent scheme, with its own energy budget, which can store liquid water in the snowpack and then simulate the refreezing of the liquid in the snowpack according to the available energy.

The water budget of the snowpack is expressed as:

$$\frac{\partial W_{snow}}{\partial t} = \frac{1}{\rho_w}(P_{snow} + p_n P_{rain} - E_{snow} - Q_n) \tag{25}$$

where W_{snow} is the snow water equivalent of the total snowpack, P_{snow} and P_{rain} are the snowfall and rainfall, respectively, E_{snow} is the sublimation of the snow, and Q_{n} is the liquid runoff from the snowpack. The snow water equivalent is split into three layers: the snow depth of the first layer is thin to simulate its fast interaction with the atmosphere. The third layer is thinner than the second one as long as the snowpack is thinner than 20 cm, so that it can interact with the soil surface, but then it becomes the thickest for deep snowpacks. Each snow layer has three prognostic variables: the snow density ρ_{snow_j}, the snow heat content H_{sj}, and the snow thickness D_{snow_j}. The snow thickness is linked to the snow water equivalent through the snow density:

$$\rho_{\text{snow}_j} D_{\text{snow}_j} = \rho_{\text{w}} W_{\text{snow}_j} \tag{26}$$

The snow density ρ_{snow_j} evolves according to the snow compaction and settling, following the expression of Anderson (1976). The density of new snow is based on the CROCUS parameterization (Brun et al., 1989), and depends on the air temperature and wind velocity, with a minimum value of 50 kg/m^3.

The snow heat content of each layer is defined using an expression similar to that of Lynch-Stieglitz (1994) and Sun et al. (1999):

$$H_{\text{sj}} = c_{\text{nj}} D_{\text{snow}_j} (T_{\text{snow}_j} - T_{\text{f}}) - L_{\text{f}} \rho_{\text{w}} (W_{\text{snow}_j} - W_{\text{snowliq}_j}) \tag{27}$$

The heat content is used to diagnose T_{snow_j} assuming there is no liquid water in the snow layer. However, if the snow layer temperature is warmer than the freezing point, T_{f}, the available energy is used to melt the snow, and the snow-layer temperature reaches T_{f} while the liquid water increases according to Eq. (27).

The liquid water in the snowpack evolves according to the incoming (R_{snow_j}) and outgoing ($R_{\text{snow}_{j-1}}$) vertical water flow (according to the water holding capacity of each snow layer), the snowmelt F_{snow_j}, and the evaporation E_{snowliq} (at the surface layer only):

$$\rho_{\text{w}} \frac{\partial W_{\text{snowliq}_j}}{\partial t} = R_{\text{snow}_{j-1}} - R_{\text{snow}_j} + \frac{F_{\text{snow}_j}}{L_{\text{f}}} - \left(\frac{W_{\text{snowliq}_j}}{W_{\text{snow}_j}} \right) E_{\text{snowliq}} \tag{28}$$

The layer-averaged snow temperature T_{snow_j} evolves according to the heat flux exchanged with the upper layer $G_{\text{snow}_{j-1}}$ and the lower layer G_{snow_j} and the liquid/solid phase changes Φ_{snow_j}:

$$c_{\text{nj}} D_j \frac{\partial T_{\text{sj}}}{\partial t} = G_{\text{snow}_{j-1}} - G_{\text{snow}_j} - \Phi_{\text{snow}_j} \tag{29}$$

The heat flux G_{snow} is the sum of the heat diffusion through the snowpack and the solar radiation absorbed by the layer (which decreases exponentially with the snow depth).

The heat flux at the snow–ground interface depends on the snow depth of the third layer and the soil–vegetation (snow-free) surface temperature T_{s}:

$$G_{\text{snow}_3} = \frac{\lambda_{\text{soil-snow}}}{\Delta z} (T_{\text{snow}_3} - T_{\text{s}}) \tag{30}$$

where $\lambda_{\text{soil-snow}}$ is a thermal conductivity computed as the average of the soil and snow thermal conductivity weighted by the thickness of the layer (half the height of the third snow layer and the soil surface layer). This flux, together with the advective term of the liquid water leaving the snowpack, constitutes the G_{snowgrnd} flux that modifies the surface temperature:

$$G_{\text{snowgrnd}} = G_{\text{snow}_3} + c_{\text{w}} R_{\text{snow}} (T_{\text{f}} - T_{\text{s}}) \tag{31}$$

The heat flux at the snow–atmosphere interface comprises the snow–surface energy budget:

$$G_{\text{snow}_0} = \epsilon_{\text{n}} (R_{\text{A}} - \sigma T_{\text{snow}_1}^4) + R_{\text{G}} (1 - \alpha_{\text{snow}}) + c_{\text{w}} p_{\text{n}} P_{\text{rain}} (T_{\text{f}} - T_{\text{a}}) - H_{\text{snow}} - \text{LE}_{\text{snow}} \tag{32}$$

The snow albedo α_{snow} decreases as a function of ageing and by the action of melt, following the parameterization of Douville et al. (1996).

The snow sensible heat flux and the snow latent heat flux LE_{snow} (which is the sum of the snow

sublimation and of the snow liquid water evaporation) are:

$$LE_s = \left[\left(1 - \frac{W_{snowl_1}}{W_{snow_1}}\right)L_s + \frac{W_{snowl_1}}{W_{snow_1}}L_v\right] \times \rho_a C_H V_a [q_{sat}(T_{snow_1}) - q_a] \quad (33)$$

$$H_s = \rho_a C_p C_H V_a (T_{snow_1} - T_a) \quad (34)$$

3. Simulation of the Torne–Kalix basin

The PILPS2(e) experiment (Bowling et al., 2003-this issue; Nijssen et al., 2003-this issue) was performed using the force-restore three-layer version of ISBA and the explicit snow scheme. In this cold climate, soil can freeze and this plays an important role in the hydrology of the area. The ISBA-FR simulation of frozen soil is limited by the actual representation of the deep soil temperature, and therefore the frozen soil depth in ISBA-FR is limited to about 30 cm. The diffusion version of ISBA has a better representation of the frozen soil processes since it is able to manage soil temperature, liquid, and solid water at each simulated level. To test the impact of a better representation of the frozen soil on the simulation of the Torne–Kalix basin, a new simulation of the PILPS2(e) domain was performed using ISBA-DF, and the comparison of the two ISBA simulation is presented in the following.

3.1. Implementation of ISBA-DF

The ISBA-DF model was calibrated for the year 1989, using the observed discharge of the Lansjaarv subbasin (see Fig. 2 of Bowling et al., 2003-this issue). The configuration chosen is a six-layer soil column, with a total soil depth comparable to the one used in PILPS2(e). The five first layer depths were set to correspond with the temperature measurement of the Abisko research station: 1, 10, 30, 80, and 120 cm everywhere in the basin, while the last soil layer thickness was set according to the vegetation type. The total soil depth is taken as 3 m for forest, 2 m for crops, and 1.5 m for grassland. The root zone depth was also set according to the same database than used in the ISBA-FR simulation, and is equal to 2 m over forest, 1.5 m over crops, and 1 m over grassland.

The ISBA-DF soil parameters were derived from the soil texture, according to the Clapp and Hornberger (1978) relationships. However, it was found that, to be able to simulate the streamflow of the Lansjaarv subbasin, the saturated hydraulic conductivity had to be reduced by a factor of 10. This parameter is known to present very large spatial variability, and a factor of 10 corresponds to one standard deviation according to Cosby et al., 1984.

The subgrid runoff produced by ISBA-DF using the same shape parameter as in PILPS2(e) increased significantly. Therefore, the shape coefficient was drastically reduced (from 0.5 to 0.1), leading to a decrease of the surface runoff production.

A deep soil temperature was imposed as a lower boundary condition (below the simulated soil column), and was set to 1 °C over the entire domain. This is actually more than the year-average air temperature (which varies between −2 and 1 °C), but a deep temperature lower than the freezing point would imply a completely frozen soil. However, as noticed by Bowling et al. (2003-this issue), permafrost occurs only on the higher part of the basin.

Also, in order to be able to make the comparison with the in situ observations, the snow was supposed to be able to entirely cover the low vegetation as soon as the snow water equivalent reached 10 mm. Indeed, a deep snow cover can efficiently isolate the soil surface from the atmosphere. In the scheme, the grid cell is assumed not to be completely homogeneous, and therefore a snow-free part of the grid cell is almost always present. This snow-free part of the grid box interacts strongly with the atmosphere, and the soil is then never entirely isolated, which can lead to very low soil temperature under extremely cold atmospheric conditions. A complete snow coverage enables the correction of such a bias, and is consistent with the conditions at the observation site.

3.2. Comparison to in situ observation of snow depth and soil temperature

A complete in situ atmospheric database has been collected over a long period of time in the Abisko research station (68.21°N, 18.49°E) (http://www.kiruna.se/forskning/ans/ans.htm). It includes measurement of

atmospheric parameters as well as snowpack and deep soil temperature. The simulation of ISBA-FR and ISBA-DF using the PILPS2(e) physiographic and atmospheric database for the grid cell corresponding to the Abisko station is compared to the in situ observations.

The comparison of the observed and simulated 10-year average (from 1989 to 1998) daily snow height is presented in Fig. 1. Accumulation of the snow tends to be 10% overestimated by the model. Snow begins to melt in March, but the melt is too fast in the models compared to the observation. It seems that parts of the error are due to differences between local atmospheric condition and grid-size PILPS2(e) forcing, since in May, while the snow continues to melt in the model, it accumulates in the observation. Then the observed snowpack disappears very quickly by the end of May, in about 2 days, while the snowmelt was slower in the model. Those observed and simulated snowpacks tend to disappear almost at the same time. There are few differences between the ISBA-FR and ISBA-DF simulations of the snowpack, since the snow height is overestimated by 2.38 and 2.53 cm by ISBA-DF and ISBA-FR, respectively. This is due to the fact that the same multilayer snow scheme is used in both simulation. The accumulation is a bit reduced in ISBA-DF due to the fact that the ground temperature is a bit warmer, thus generating higher exchange between the snowpack and the ground.

Comparison of the 10-year simulated and observed daily soil temperatures is presented in Fig. 2. The soil temperature simulated by ISBA-DF corresponds to the depth of the observation, while for ISBA-FR, only the simulated surface soil temperature corresponds to a depth of 5 cm. The deep soil temperature is closer to 30 cm, and is then compared to the 20 and 50 cm observed soil temperature. Clearly, the simulation of soil temperature is improved by ISBA-DF compared to ISBA-FR, with an underestimation of the temperature from 1 to 0.1 °C at 5 and 50 cm, while this bias reaches − 5.6 and − 5.3 °C for ISBA-FR. The annual cycle is also better represented by ISBA-DF than by ISBA-FR, with a square correlation coefficient ranging from 1 at 5 cm to 0.7 at 50 cm. However, a phasing problem appears at 50 cm, and is more pronounced at 100 cm, with a maximum soil temperature observed in September and simulated in mid-July, resulting to a poor square correlation (0.4), while the bias remains low (− 0.2 °C). This problem may be link to the restore temperature, which smoothes the cycle of the deep temperature. It may also be due to a change of the soil properties with depth, or to an interaction with a water table. However, as no observed data were available to go further in the

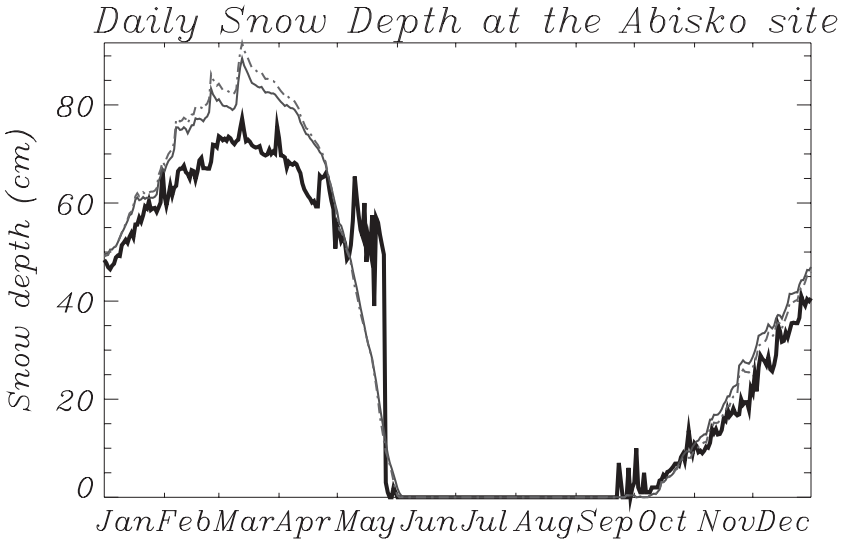

Fig. 1. Comparison between the 10-year averaged (1989–1998) daily snow depth observed at the Abisko research station (thick line), simulated by ISBA-FR (dotted line) and by ISBA-DF (thin line).

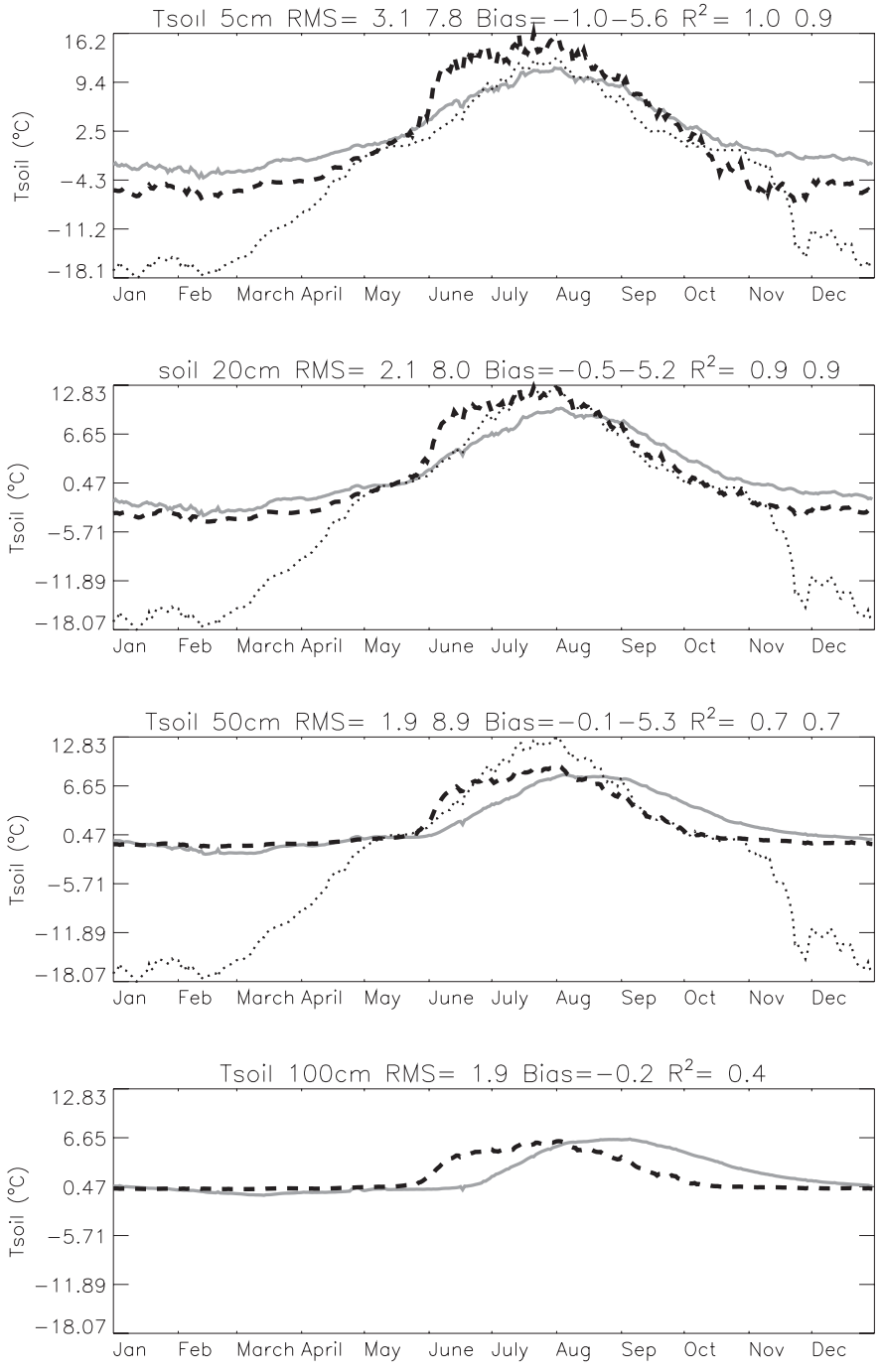

Fig. 2. Comparison between the 10-year averaged (1989–1998) daily soil temperatures observed at the Abisko research station (plain line), simulated by ISBA-DF (thin line) and by ISBA-FR (dotted line). The observation depths are 5, 20, 50, and 100 cm. Statistical results are indicated on the title, RMS stands for root mean square, and R^2 for the square correlation; first numbers are for ISBA-DF, and then for ISBA-FR if available.

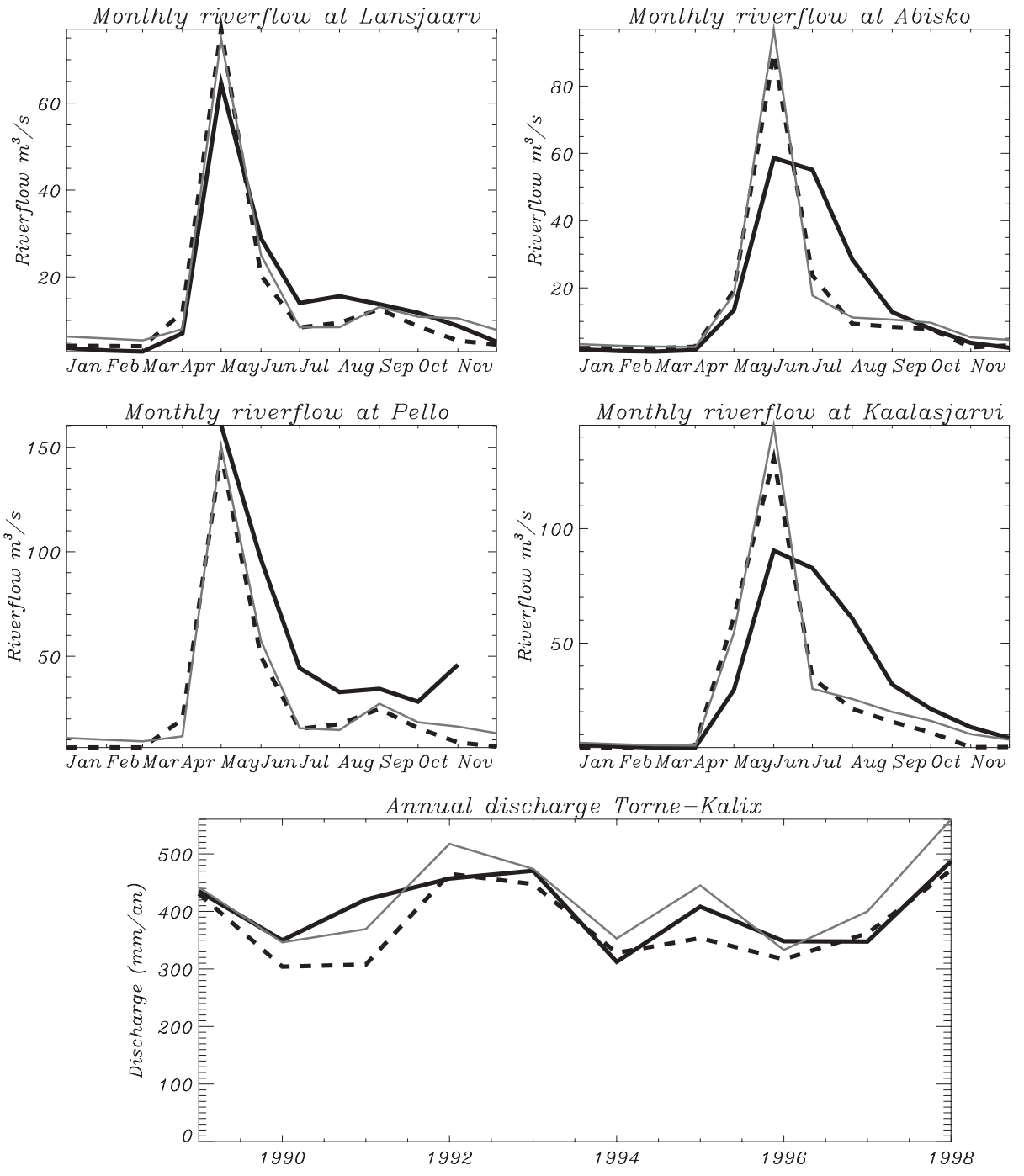

Fig. 3. Comparison between the 10-year averaged (1989–1998) monthly streamflow of the Lansjaarv, Abisko, Pello, and Kaalasjarvi subbasins, and with the annual discharge of the whole Torne–Kalix basin. Observations are in thick line, and simulations by ISBA-DF and ISBA-FR are in thin line and dotted line, respectively.

analysis, a homogenous texture profile was used over the soil column, and no gradient of the soil water potential is supposed at the bottom of the soil column.

3.3. Comparison to observed streamflows

The comparison of the 10-year averaged monthly observed and simulated riverflows at the Lansjaarv, Abisko, Pello, and Kaalasjarvi subbasins is presented in Fig. 3, and the statistical results are presented in Table 1. The two subbasins below the tree lines (Lansjaarv and Pello) are better simulated than the two subbasins above the tree line (Abisko and Kaalasjarvi). The main problem is an important overestimation of the peaks in spring. This may be due to a large overestimation of the snowmelt. The comparison with the available observed snow depth at the research station of Abisko presents such a defect, but not to such an extent since the snow height is only overestimated by 10%, and the snow disappears at about the same time in the observation and simulation. Another reason for the overestimation is that in these two subbasins, during the snowmelt, part of the runoff is stored in some lakes that are still frozen, adding a time delay before the water actually reaches the river. This phenomenon was taken into account by very few schemes in the PILPS2e experiments, either by using a lake scheme (MATSIRO) or by calibrating some time transfer coefficient as in VIC (see Bowling et al., 2003-this issue). However, this phenomenon was not taken into account in ISBA, which was unable to correctly simulate the discharge of these subbasins.

Table 1
Statitiscal results obtained by ISBA-FR and ISBA-DF on the simulation of the monthly riverflows of the Lansjaarv, Abisko, Pello, and Kaalasjarvi subbasins, as well as on the discharge of the whole Torne–Kalix catchment

River	Q_{sim}/Q_{obs}		E		R^2	
	ISBA-FR	ISBA-DF	ISBA-FR	ISBA-DF	ISBA-FR	ISBA-DF
Lansjaarv	0.95	1.03	0.90	0.93	0.96	0.95
Abisko	0.04	1.10	0.50	0.33	0.66	0.59
Pello	0.62	0.68	0.69	0.77	0.91	0.93
Kaalasjarvi	0.84	0.93	0.35	0.27	0.57	0.55
Torne–Kalix	0.94	1.05	0.39	0.47	0.67	0.75

Q_{sim}/Q_{obs} is the ratio of the simulated versus observed discharge, E is the efficiency, and R^2 is the square correlation coefficient.

The riverflow of the Torne and Kalix riverflow were simulated during the PILPS2(e) experiment using a routing model, which takes into account the deviation of the Kalix to the Torne (Bowling et al., 2003-this issue). Without such a routing model, it is possible to compare the observed and simulated annual discharge of the Torne and Kalix basins associated, which is presented in Fig. 3. The annual discharge is underestimated by 6% by ISBA-FR and overestimated by 5% by ISBA-DF, with a better correlation for ISBA-DF ($R^2 = 0.75$) compared to ISBA-FR ($R^2 = 0.67$).

Thus, even if some differences appear between the riverflow simulations of ISBA-DF and ISBA-FR (mainly during the low flow, in wintertime), the results of both model are quite close. These small differences can be due to the fact that both models share the same description of the snowpack, and that snowmelt is the main contributor of the riverflow in this region.

3.4. Comparison of the ISBA-FR and ISBA-DF simulations

The ISBA-FR simulation submitted for the PILPS2e experiment differs from the present ISBA-DF simulation mainly through the representation of the processes in the soil column, and also, as it was said earlier, by the coverage of the snowpack: for a low vegetation type, in ISBA-DF, the snow is supposed to cover entirely the cell. This has no impact in the forested area as in Lansjaarv, but leads to a bit longer snow duration in the northern part of the basin covered by low vegetation (Fig. 4). However, more importantly, as the surface is completely covered by snow, the surface albedo is higher, which leads to a general decrease of the net radiation (-4.5 W/m^2). Consistent with the vegetation being buried a longer time by the snow, the evaporation, and especially, the transpiration decreased (-2.25 W/m^2 and -28 mm, respectively). As the surface temperature tends to be warmer in DF than in FR, the sensible heat flux decreases (-3.7 W/m^2), and the ground heat flux increases ($+3.0$ W/m^2).

Comparison of the liquid and solid water profiles (Fig. 4) shows that the soil ice melts earlier in ISBA-FR than in ISBA-DF (due to the warming in spring from the snow-free part of the cell in ISBA-FR). In

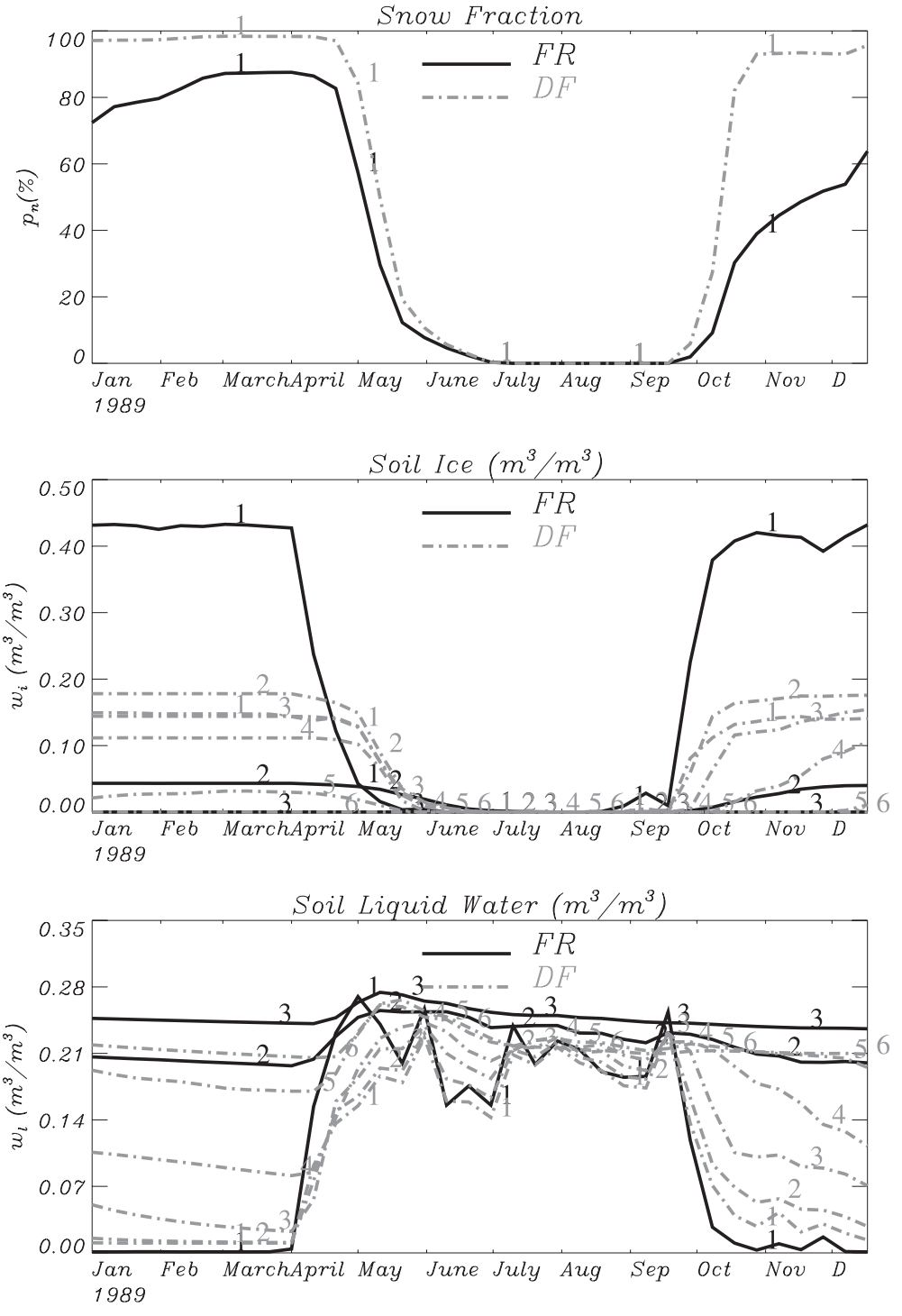

Fig. 4. Comparison of the ISBA-DF (dotted line) and ISBA-FR (plain line) simulations of the 10-day averaged soil ice and liquid content for each simulated layers, averaged over the entire Torne basin. The numbers correspond to the layer index.

ISBA-DF, the three first layers are almost entirely frozen in wintertime, while the fourth layer is only partially frozen. There are few available observations of the frozen soil depth. One observation site, in the northwestern part of the basin (20.61°E, 69.04°N), measured a frozen soil depth that varies from 9 to 45 cm, with an average value of 24.3 cm (Bowling, personal communication). At this site, the frozen soil depth simulated by ISBA-FR is 20 cm in average, and varies from 0 to 35 cm, while the averaged soil depth simulated by ISBA-DF is 24 cm, and ranges from 0 to 45 cm. Over the whole basin, in wintertime, there is very low spatial variation of the frozen soil depth simulated by ISBA-FR (about 30 cm), while it varies from 90 to 20 cm in ISBA-DF, which seems more realistic.

4. Conclusion

The latest developments made on the soil and snow modules of the ISBA surface scheme are briefly summarized in this article. Mainly, the explicit snow scheme allows to have a separate energy budget for the snow and snow-free part of the cell, and to simulate some important processes as the storage and freezing of liquid water in the snowpack. The frozen soil parameterization and the third hydrologic layer of the force-restore version of ISBA made it possible to separate the root zone layer from a deep, hydrological active soil layer, and to take into account the energy flux due to liquid/solid water phase transfer. The new diffusion soil module is a step forward, since a vertical profile of soil temperature, liquid, and solid water can be simulated. The application of the soil diffusion scheme over the PILPS2(e) area tends to show that ISBA-DF performs well in terms of both hydrology and soil temperature. Comparison of ISBA-DF with observation of streamflow over five subbasins, and with soil temperature and snow depth at the Abisko research station site, has shown a fairly good agreement.

Acknowledgements

We would like to thank Laura Bowling, Bart Nijssen, and Dennis Lettenmaier for the meaningful work they made for the PILPS2(e) experiment, with a special attention to Laura who where always very friendly and helpful while answering numerous questions. We would also like to thank the Swedish Meteorological and Hydrological Institute for delivering their data. Many thanks are given to Per-Erik Jansson, from the Royal Institute of technology in Stockholm, which provided very good advices. Also, we would like to thank the reviewers for their useful comments and help for improving this article.

Appendix A

List of symbols

α	surface albedo
ϵ	surface emissivity
λ	thermal conductivity (J s^{-1} m^{-1} K^{-1})
ρ_a	air density (kg m^{-3})
ρ_w	water density (kg m^{-3})
σ	Stefan Boltzmann cst (J m^{-2} s^{-1} K^{-4})
τ	time period of 1 day (s)
C_G	soil thermal coefficient (m^2 K J^{-1})
C_p	specific heat of air (J kg^{-1} K^{-1})
C_H	drag coefficient
C_1, C_2, C_4	force-restore coefficients for soil moisture
C_3	coefficient for gravitational drainage
L_f	latent heat of fusion (J kg^{-1})
L_v	latent heat of vaporisation (J kg^{-1})
L_s	latent heat of sublimation (J kg^{-1})
P_g	precipitation rate that reaches the ground (kg/m^2/s)
T_a	air temperature (K)
V_a	wind speed (m s^{-1})
c_g	volumetric heat capacity (J K^{-1} m^{-3})
c_i	volumetric heat capacity of the soil ice (J K^{-1} m^{-3})
c_{nj}	volumetric heat capacity of the snow (J K^{-1} m^{-3})
c_w	volumetric heat capacity of the water (J K^{-1} m^{-3})
d_1	surface soil depth (m)
d_2	root zone depth (m)
d_3	total soil depth (m)
h_u	liquid relative humidity at the ground surface
h_{ui}	ice relative humidity at the ground surface
q_a	air specific humidity (kg/kg)

q_{sat} saturated specific humidity (kg/kg)
w_{fc} field capacity (m^3/m^3)
w_{sat} saturated soil moisture (m^3/m^3)
w_{l1eq} liquid soil moisture at equilibrium (m^3/m^3)

References

Anderson, E.A., 1976. A point energy and mass balance model of a snow cover. NOAA Tech. Rep. NWS 19. U.S. Dept. of Commer., Washington, DC, 150 pp.

Boone, A., 2000. Modélisation des processus hydrologiques dans le schéma de surface ISBA: Inclusion d'un réservoir hydrologique, du gel et modélisation de la neige. PhD thesis, Université Paul Sabatier, Toulouse.

Boone, A., Etchevers, P., 2001. An inter-comparison of three snow schemes of varying complexity coupled to the same land-surface and macroscale hydrologic models. Part I: local scale evaluation at an alpine site. J. Hydrometeorol. 2, 374–394.

Boone, A., Calvet, J.-C., Noilhan, J., 1999. Inclusion of a third soil layer in a land surface scheme using the force restore method. J. Appl. Meteorol. 38 (11), 1611–1630.

Boone, A., Masson, V., Meyers, T., Noilhan, J., 2000. The influence of the inclusion of soil freezing on simulations by a soil–atmosphere-transfer scheme. J. Appl. Meteorol. 39, 1544–1569.

Boone, A., Habets, F., Noilhan, J., 2001. The Rhone-aggregation experiment. GEWEX News 11 (3), 3–5.

Bowling, L., Lettenmaier, D., Nijssen, B., Graham, P., Clark, D., El Maayar, M., Essery, R., Goers, S., Habets, F., Van der Hurk, B., Jing, J., Kahan, D., Lohmann, D., Mahanama, S., Mocko, D., Nasonova, O., Samuelsson, P., Shmakin, A., Takata, K., Verseghy, D., Viterbo, P., Xieyao, M., Xue, Y.K., Yang, Z.L., 2003. Simulation of high latitude hydrological processes in the Torne–Kalix basin: PILPS phase 2(e) 1: Experiment description and summary intercomparisons. Glob. Planet. Change 38, 1–30.

Braud, I., Noilhan, J., Bessemoulin, P., Mascart, P., Haverkamp, R., Vauclin, M., 1993. Bare-ground surface heat and water exchanges under dry conditions: observations and parameterization. Boundary-Layer Meteorol. 66, 173–200.

Brooks, R.H., Corey, A.T., 1966. Properties of porous media affecting fluid flow. J. Irrig. Drain. Am. Soc. Civil Eng. IR2, 61–88.

Brun, E., Martin, E., Simon, V., Gendre, C., Coléou, C., 1989. An energy and mass model of snow cover suitable for operational avalanche forecasting. J. Glaciol. 35 (121), 333–342.

Calvet, J.-C., 2000. Investigating soil and atmospheric plant water stress using physiological and micrometeorological data sets. Agric. For. Meteorol. 103, 229–247.

Calvet, J.-C., Noilhan, J., Roujean, J.-L., Bessemoulin, P., Cabelguenne, M., Olioso, A., Wigneron, J.-P., 1998. An interactive vegetation SVAT model tested against data from six contrasting sites. Agric. For. Meteorol. 92, 73–95.

Clapp, R.B., Hornberger, G.M., 1978. Empirical equations for some hydraulic properties. Water Resour. Res. 14, 601–604.

Cosby, B.J., Hornberger, G.M., Clapp, R.B., Ginn, T.R., 1984. A statistical exploration of the relationships of soil moisture characteristics to the physical properties of soil. Water Resour. Res. 20, 682–690.

Douville, H., Royer, J.F., Mahfouf, J.F., 1996. A new snow parameterization for the Météo France climate model. Clim. Dyn. 12, 21–52.

Etchevers, P., Golaz, C., Habets, F., 2000. Simulation of the water budget and the river flows of the Rhone basin from 1981 to 1994. J. Hydrol. 244, 60–85.

Fuchs, M., Campbell, G.S., Papendick, R.I., 1978. An analysis of sensible and latent heat flow in a partially frozen unsaturated soil. Soil. Sci. Soc. Am. J. 42, 379–385.

Giard, D., Bazile, E., 2000. Implementation of a new assimilation scheme for soil and surface variables in a global NWP model. Mon. Weather Rev. 128, 997–1015.

Habets, F., Noilhan, J., Golaz, C., Goutorbe, J.P., Lacarrre, P., Leblois, E., Ledoux, E., Martin, E., Ottlé, C., Vidal-Madjar, D., 1999a. The ISBA surface scheme in a macroscale hydrological model, applied to the HAPEX-MOBILHY area: part 1 model and data base. J. Hydrol. 217, 75–96.

Habets, F., Etchevers, P., Golaz, C., Leblois, E., Ledoux, E., Martin, E., Noilhan, J., Ottlé, C., 1999b. Simulation of the water budget and the river flows of the Rhone basin. J. Geophys. Res. 104, 31145–31172.

Lynch-Stieglitz, M., 1994. The development and validation of a simple snow model for the GISS GCM. J. Climate 7, 1842–1855.

Masson, V., 2000. A physically-based scheme for the urban energy budget in atmospheric models. Boundary-Layer Meteorol. 94, 357–397.

Nijssen, B., Bowling, L., Lettenmaier, D., Clark, D., El Maayar, M., Essery, R., Goers, S., Habets, F., Van der Hurk, B., Jing, J., Kahan, D., Lohmann, D., Mahanama, S., Mocko, D., Nasonova, O., Samuelsson, P., Shmakin, A., Takata, K., Verseghy, D., Viterbo, P., Xia, Y., Xieyao, M., Xue, Y.K., Yang, Z.L., 2001. Simulation of high latitude hydrological processes in the Torne–Kalix basin: PILPS Phase 2(e) 2: Comparison of model results with observation. Glob. Planet. Change 38, 31–53.

Noilhan, J., Mahfouf, J.-F., 1996. The ISBA land surface parameterization scheme. Glob. Planet. Change 13, 145–159.

Noilhan, J., Planton, S., 1989. A simple parameterization of land surface processes for meteorological models. Mon. Weather Rev. 117, 536–549.

Sun, S.J., Jin, J., Xue, Y., 1999. Simple snow–atmosphere–soil transfer (SAST) model. J. Geophys. Res. 104, 19587–19597.

Wood, E., Lettenmaier, D., Zartarian, V., 1992. A land-surface hydrology parameterization with subgrid variability for general circulation models. J. Geophys. Res. 97, 2717–2728.